Supporting Information

Na et al. 10.1073/pnas.1407780111

SI Materials and Methods

Composition Dependence of Glass-Forming Ability. Series I–IV of the alloy family $Ni_{100-w-x-y-z}Cr_wNb_xP_yB_z$ are as follows: $Ni_{77.5-w}Cr_wNb_3P_{16.5}B_3$ (series I), $Ni_{69}Cr_{11.5-x}Nb_xP_{16.5}B_3$ (series II), $Ni_{69}Cr_{8.5}Nb_3P_{19.5-z}B_z$ (series III), and $(Ni_{0.8541}Cr_{0.1085}Nb_{0.0374})_{100-(y+z)}(P_{0.8376}B_{0.1624})_{(y+z)}$ (series IV). The eutectic composition is $Ni_{69}Cr_{8.5}Nb_3P_{16.5}B_3$, and hence the transition from hypo- to hypereutectic occurs at $w = 8.5$, $x = 3$, $z = 3$, and $(y + z) = 19.5$, for series I–IV, respectively.

The d_{cr} vs. composition data presented in Fig. 4 for series I–IV are fitted using an exponential fitting function, as follows:

$$d_{cr} = a\exp(b\mathbf{c}) + d. \qquad \textbf{[S1]}$$

The fitting coefficients a, b, and d for series I–IV are presented in Table S1 for the corresponding hypo- and hypereutectic regions. The composition variable $\mathbf{c}$ is in units of w, x, z, and $(y + z)$, for series I–IV, i.e., in atomic percentages of Cr, Nb, B, and total metalloid (i.e., combined P and B). d_{cr} is presented in millimeters.

The d_{cr}^2 vs. B concentration data presented in Fig. 5*A* for $Ni_{69}Cr_{8.5}Nb_3P_{19.5-z}B_z$ (series III) are fitted using the exponential fitting function.

$$d_{cr}^2 = a\exp(b\mathbf{c}). \qquad \textbf{[S2]}$$

The composition variable $\mathbf{c}$ is in units of z, i.e., in atomic percentages of B, and d_{cr}^2 in millimeters squared. The fitting coefficients a and b are 800 and −0.693, respectively.

Calorimetry. Differential scanning calorimetry was performed to evaluate the glass transition temperature T_g, crystallization temperature T_x, solidus temperature T_S, and liquidus temperature T_L for $Ni_{69}Cr_{8.5}Nb_3P_{19.5-z}B_z$ (series III) metallic glass alloys for z between 1.5 and 6. T_g and T_x were evaluated as the onset of the glass transition at a scan rate of 20 K/min. T_S and T_L were evaluated at a scan rate of 5 K/min to reduce scan rate effects and instrumental broadening of the melting transition. Scans around the glass transition are presented in Fig. S1, and around the melting transition are presented in Fig. S2. Data for T_g, T_x, T_S, T_L, and t_{rg} are presented in Table S2.

Rheometry. The equilibrium (Newtonian) viscosity for $Ni_{69}Cr_{8.5}Nb_3P_{19.5-z}B_z$ (series III) metallic glass alloys for $z = 1.5$, 3, and 5 was measured by performing three-point beam bending of amorphous rods 2 mm in diameter and 10 mm in length using a thermomechanical analyzer (Perkin–Elmer; TMA 7), as described by Hagy (1). Specifically, the isothermal viscosity at a given temperature is determined by the following equation:

$$\eta = -\frac{g\ L^3}{144 I_c \nu}\left(M + \frac{5\rho A L}{8}\right), \qquad \textbf{[S2]}$$

where η is the apparent viscosity (Pa·s), g the gravitational constant (meters per second squared), L the support span length (meters), I_c the cross-sectional moment of inertia (meters to the fourth power), ν the midpoint deflection velocity (meters per second), M the applied load (kilograms), ρ the density (kilograms per meter cubed), and A is the cross-sectional area (meters squared). Loads ranging from 20 to 1,000 mN were applied. Measured data for $Ni_{69}Cr_{8.5}Nb_3P_{18}B_{1.5}$, $Ni_{69}Cr_{8.5}Nb_3P_{16.5}B_3$, and $Ni_{69}Cr_{8.5}Nb_3P_{14.5}B_5$ are presented in Fig. S3.

To describe the temperature dependence of viscosity $\eta(T)$, the cooperative shear model is used (2, 3):

$$\frac{\eta(T)}{\eta_\infty} = \exp\left\{\frac{W_g}{kT}\exp\left[2n\left(1 - \frac{T}{T_{go}}\right)\right]\right\}, \qquad \textbf{[S3]}$$

where η_∞ is the high-temperature limit of viscosity, which is assumed to be 10^{-3} Pa·s for all alloys, W_g is the activation energy barrier at the glass transition, approximated by $W_g \approx kT_{go}\log(\eta_g/\eta_\infty)$, where $\eta_g \equiv 1\times10^{12}$ Pa·s, n is the effective fragility parameter, k the Boltzmann constant, T temperature, and T_{go} the glass transition temperature associated with a viscosity value of 10^{12} Pa·s. The fragility parameter m is related to n via

$$m = (1 + 2n)\log(\eta_g/\eta_\infty). \qquad \textbf{[S4]}$$

The fitting curves for $Ni_{69}Cr_{8.5}Nb_3P_{18}B_{1.5}$, $Ni_{69}Cr_{8.5}Nb_3P_{16.5}B_3$, and $Ni_{69}Cr_{8.5}Nb_3P_{14.5}B_5$ are presented in Fig. S3, whereas the fit parameters T_{go} and n and the calculated fragility m are given in Table S3.

Mathematical Analysis. The actual dependence of $\ln\tau_\alpha^*(\mathbf{c})$ on W and ΔG_α depends on the theoretical model used to describe these barriers. In this analysis, we assume only that $\ln\tau_\alpha^*(\mathbf{c})$ is a well-behaved function of composition that depends on the dimensionless parameters t_{rg}, m, and any other potentially relevant material parameters (e.g., the interfacial free energy, $\sigma_{L\alpha}$, of the liquid–crystal interface). In other words we take $\ln\tau_\alpha^*(\mathbf{c}) = \ln[f(\boldsymbol{c},\ t_{rg}, m, \sigma_{L\alpha}, \ldots)]$, where f is an unknown function of the parameters $t_{rg}(\boldsymbol{c})$, $m(\boldsymbol{c})$, etc. that are themselves functions of composition.

For a 1D composition variation z as in our alloy series, the compositional derivative of lnf [where $f = \tau_\alpha^*(\mathbf{c})$] for α-crystallization becomes

$$\frac{dlnf}{dz} = \frac{1}{f}\frac{df}{dz} + \frac{1}{f}\left[\frac{df}{dt_{rg}}\frac{dt_{rg,\alpha}}{dz} + \frac{df}{dm}\frac{dm}{dz} + \frac{df}{d\sigma_{L\alpha}}\frac{d\sigma_{L\alpha}}{dz} + \ldots\right]. \qquad \textbf{[S5]}$$

The first term on the right includes any explicit dependence of f on composition not described by our parameters. For a model of crystal nucleation, this term can be assumed to vanish because the independent parameters taken together with their dependence on z and T are assumed to give a full description of the nucleation rate. The series expansion of Eq. **S5** along the z direction then becomes to first order:

$$\ln\left(f(z)_\alpha\right) = \ln\left(f(z_0)_\alpha\right) + \left[\frac{df}{dt_{rg}}\frac{dt_{rg,\alpha}}{dz} + \frac{df}{dm}\frac{dm}{dz} + \frac{df}{d\sigma_{L\alpha}}\frac{d\sigma_{L\alpha}}{dz} + \ldots\right]_{z_0}(z - z_0), \qquad \textbf{[S6]}$$

Referring to Eq. **S6**, one sees that the term in the square bracket can be identified as the z component of the $\boldsymbol{\lambda_\alpha}$ vector, where $z = \boldsymbol{\lambda_\alpha}\cdot(\boldsymbol{c} - \boldsymbol{c}_0)$. Further, one observes that the $\boldsymbol{\lambda_\alpha}$ for the alloy series naturally separates into contributions arising from each independent variable t_{rg}, m, etc. We write:

$$\lambda_\alpha = \lambda_{t_{rg,\alpha}} + \lambda_{m,\alpha} + \ldots, \qquad \textbf{[S7]}$$

where $\lambda_{t_{rg,\alpha}} = (df/dt_{rg})(dt_{rg,\alpha}/dz)$, $\lambda_{m,\alpha} = (df/dm)(dm/dz)$, etc. for each independent parameter. Eq. **S7** is essentially Eq. **3a** for analyzing the glass-forming ability (GFA) cusp.

One may separate the exponential dependence of GFA on composition into contributions associated with each independent parameter in a nucleation model. We may use this property to analyze experimental GFA data for our alloy series. Because t_{rg}, m, etc. are experimentally accessible material properties that are composition dependent, one can measure the derivatives, $dt_{rg,\alpha}/dz$, dm/dz, etc. Our GFA composition data provide experimental values of the total λ_α. For a cusp composition (i.e., the eutectic composition), we have two separate equations associated with hypo- and hypereutectic crystallization pathways thereby obtaining two sets of these equations at the same value of z_o. These coupled equations may be solved to obtain the derivatives, df/dt_{rg}, df/dm, etc. These are theoretical quantities that depend on the model used to describe crystal nucleation. Using this analysis along with relevant experimental data, we show that the composition dependence of GFA in the present Ni-based alloys arises mainly from the composition dependence of the two parameters t_{rg} and m.

1. Hagy HE (1963) Experimental evaluation of beam bending method of determining glass viscosities in the range 10^8 to 10^{15} Poise. *J Am Ceram Soc* 46(2):93–97.
2. Demetriou MD, et al. (2006) Cooperative shear model for the rheology of glass-forming metallic liquids. *Phys Rev Lett* 97(6):065502.
3. Johnson WL, Demetriou MD, Harmon JS, Lind ML, Samwer K (2007) Rheology and ultrasonic properties of metallic glass forming liquids: A potential energy landscape perspective. *MRS Bull* 32(1-2):644–650.

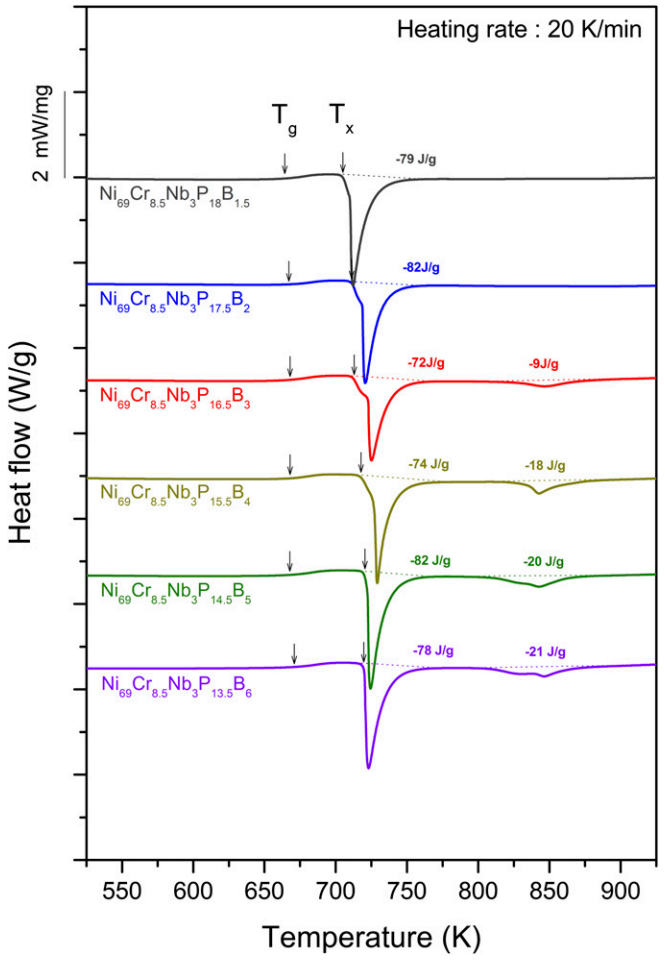

Fig. S1. Calorimetry scans around the glass transition for $Ni_{69}Cr_{8.5}Nb_3P_{19.5-z}B_z$ (series III) metallic glass alloys with z between 1.5 and 6. Arrows designate the glass transition temperature (left arrow) and crystallization temperature (right arrow). The enthalpies of crystallization are also noted in the plot.

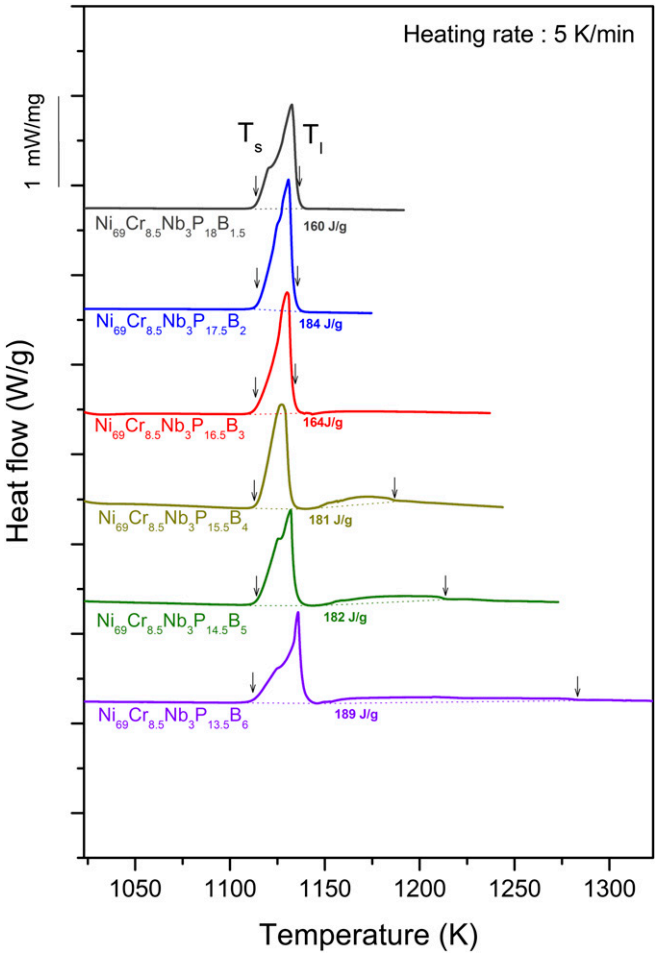

Fig. S2. Calorimetry scans around the melting transition for $Ni_{69}Cr_{8.5}Nb_3P_{19.5-z}B_z$ (series III) metallic glass alloys with z between 1.5 and 6. Arrows designate the solidus temperature (left arrow) and liquidus temperature (right arrow). The enthalpies of melting are also noted in the plot.

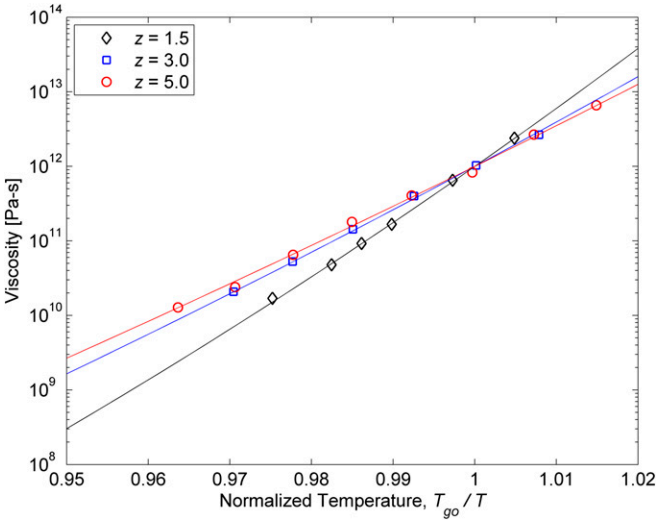

Fig. S3. Data and fitting curves for the equilibrium viscosity of $Ni_{69}Cr_{8.5}Nb_3P_{19.5-z}B_z$ (series III) metallic glass alloys with z = 1.5, 3, and 5.

Table S1. Fitting coefficients to GFA vs. composition data according to Eq. S1 for series I–IV alloys

	Hypoeutectic			Hypereutectic		
Alloy series	*a*	*b*	*d*	*a*	*b*	*d*
Series I	0.0724	0.511	4.44	293	−0.439	4.38
Series II	2.25	0.566	−2.26	851	−1.59	2.69
Series III	0.212	1.17	2.74	32.9	−0.474	2.05
Series IV	2.73×10^{-5}	0.654	0.464	5.61×10^{5}	−0.550	0

Table S2. Glass transition temperature T_g, crystallization temperature T_x, solidus temperature T_S, liquidus temperature T_L, and Turnbull parameter t_{rg} for series III alloys

Alloy	T_g, K	T_x, K	T_S, K	T_L, K	t_{rg}
$Ni_{69}Cr_{8.5}Nb_3P_{18}B_{1.5}$	664	705	1114	1134	0.5856
$Ni_{69}Cr_{8.5}Nb_3P_{17.5}B_2$	667	711	1114	1134	0.5882
$Ni_{69}Cr_{8.5}Nb_3P_{16.5}B_3$	668	713	1114	1134	0.5891
$Ni_{69}Cr_{8.5}Nb_3P_{15.5}B_4$	668	720	1113	1187	0.5628
$Ni_{69}Cr_{8.5}Nb_3P_{14.5}B_5$	668	721	1114	1214	0.5505
$Ni_{69}Cr_{8.5}Nb_3P_{13.5}B_6$	671	720	1112	1285	0.5222

Table S3. Fit parameters T_{go} and n and calculated fragility m for series III alloys

Alloy	T_{go}, K	n	m
$Ni_{69}Cr_{8.5}Nb_3P_{18}B_{1.5}$	661.2	2.05	76.5
$Ni_{69}Cr_{8.5}Nb_3P_{16.5}B_3$	653.1	1.46	58.9
$Ni_{69}Cr_{8.5}Nb_3P_{14.5}B_5$	667.8	1.30	54.0